Journal of Energy Storage xxx (xxxx) xxx

Contents lists available at ScienceDirect

Journal of Energy Storage

journal homepage: www.elsevier.com/locate/est

Morphology controlled synthesis of battery-type $NiCo_2O_4$ supported on nickel foam for high performance hybrid supercapacitors

Doan Tien Phat [a], Pham Manh Thao [a], Nguyen Van Nghia [b,c], Luong Trung Son [a], Tran Viet Thu [a], Ngo Thi Lan [a], Ngo Quy Quyen [a], Nguyen Van Ky [a], To Van Nguyen [a,*]

[a] Department of Chemical Engineering, Le Quy Don Technical University, Hanoi, 100000, Viet Nam
[b] Research Center of Advanced Materials and Applications, Institute of Architecture, Construction, Urban and Technology, Hanoi Architectural University, Hanoi, 100000, Viet Nam
[c] Department of Physics, Open Training Institute, Hanoi Architectural University, Hanoi, 100000, Viet Nam

ARTICLE INFO

Keywords:
Hydrothermal synthesis
Hybrid supercapcitors
Battery-type
$NiCo_2O_4$
High performance

ABSTRACT

In this study, we successfully synthesized $NiCo_2O_4$ supported on Ni foam (NNCOs) with different morphologies by changing the synthesis conditions. The research results of electrochemical properties show that the morphologies have a strong influence on the electrochemical properties of materials. Specifically, the nanosheet-like NNCO-1 sample exhibited an enhanced specific capacity of 503.5 C g^{-1} at current density of 1 A g^{-1}, *ca.* 134-350 % higher than that of NNCO-2, NNCO-4 (nanorod-like) and NNCO-3 (grass-like). All materials also show high stability with the ability to maintain 95 to 97% capacitance after 2000 discharge cycles at a current density of 2 A g^{-1}. We hope that, the NNCO-1 material is promising electrode material for hybrid supercapacitor.

1. Introduction

Today, the strong development of electronic technology has imposed higher requirements for energy storage sources such as: high durability, high energy density, high power density, safety, smaller size, and lower weight...[1,2]. Among the energy storage devices, chemical batteries with high energy density and supercapacitors with high power density are the most potential devices [3,4]. However, the low power density in chemical battery and the small energy density in supercapacitors are the biggest disadvantage in practical application [5–7]. An effective solution to resolve this problem is the research and development hybrid supercapacitors, which are energy storage devices based on both the energy storage mechanism of chemical battery and energy storage mechanism of supercapacitor [8,9]. Typically, hybrid supercapacitors include of a capacitor-type electrode and a battery-type electrode so that it takes full advantage of high energy density of battery and high power density of the supercapacitor [9–11].

Battery-type materials in hybrid supercapacitors are usually transition metal oxides and conductive polymers [12–14]. Compared to conductive polymers, transition metal oxides are more commonly used because of their high stability, low cost, and in particular they have many valence states [15]. Among transition metal oxides, spinel-type metal oxides (AB_2O_4) have received intensive attention as a promising electrode materials for hybrid supercapacitor [16–19]. One of the most popular spinel-type metal oxides is $NiCo_2O_4$ because it has a much greater energy storage capacity than other spinel-type metal oxides. It has been reported that flower-like $NiCo_2O_4$ directly applied as electrodes for hybrid supercapacitors show maximum specific capacity of 120 C/g at current density of 2 A/g [14]. In addition, Ju Fang and co-workers reported about $NiCo_2O_4$ with morphology nanosheet-like for application in hybrid supercapacitors [20], the result shows that materials exhibited behaviors of battery-type with maximum specific capacity of 372 C g^{-1} at 1 A g^{-1}. As another example, maximum specific capacity of $NiCo_2O_4$ hollow spheres [21], $NiCo_2O_4$ microspheres [22] are 171.2 and 202 C g^{-1} at 1 A g^{-1}. It can be seen that, the above studies mainly focused on different solutions to obtain $NiCo_2O_4$ with high electrochemical efficiency and showing that the morphology has a strong influence on the electrochemical properties of the material. Moreover, the material obtained requires extra the electrode preparation process before investigate the electrochemical. Therefore, synthesizing $NiCo_2O_4$ supported on conductive collector and studying the influence of morphology to their electrochemical properties is very meaningful.

In this study, we report on a hydrothermal method for synthesis

* Corresponding author.
E-mail address: tptnhv@gmail.com (T. Van Nguyen).

https://doi.org/10.1016/j.est.2020.102030
Received 20 July 2020; Received in revised form 30 September 2020; Accepted 26 October 2020

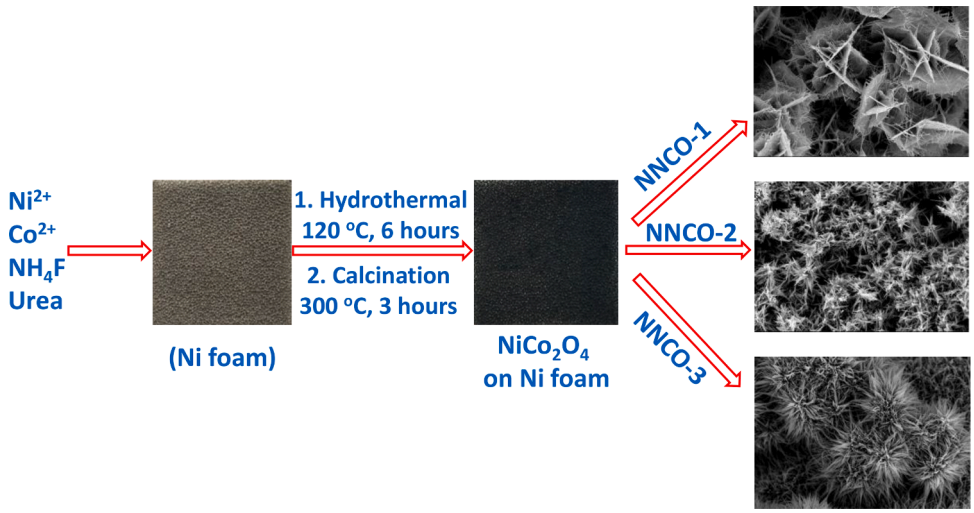

Fig. 1. Synthesis flowchart for the $NiCo_2O_4$ materials supported on Ni foam.

Table 1
Ratio between precursor chemicals for different samples.

	Amount (mmol)			
	$NiCl_2.6H_2O$	$CoCl_2.6H_2O$	Urea	NH_4F
NNCO-1	0.5	1	7.5	3
NNCO-2	0.75	1.5	11.25	4.5
NNCO-3	1	2	15	6
NNCO-4	0.5	1	11.25	3

$NiCo_2O_4$ supported on Ni foam with different morphologies by varying the concentration of reaction precursors. The results indicated that $NiCo_2O_4$ is prepared at different concentrations of the precursors, resulting in different morphologies such as nanosheet-like (NNCO-1), nanowire-like (NNCO-2, NNCO-4) and urchin-like (NNCO-3). We found that, all $NiCo_2O_4$ samples showed battery-type behavior and electrochemical performance depending on their morphology. Specifically, $NiCo_2O_4$ with the morphology as nanosheet-like has shown specific capacity more impressively than $NiCo_2O_4$ with other morphologies.

2. Experimental

2.1. Chemicals

Ni foam, Urea, Ammonium fluoride (NH_4F), Nickel (II) Chloride hexahydrate ($NiCl_2.6H_2O$), Cobalt (II) Chloride hexahydrate ($CoCl_2.6H_2O$), Acetylene black (AB), Poly(vinylidene fluoride) (PVDF), N-methyl pyrrolidone (NMP). All chemicals were purchased from Shanghai Aladdin Bio-Chem Technology Co.Ltd.

2.2. Materials synthesis

$NiCo_2O_4$ supported on Ni foam were fabricated through a simple hydrothermal growth together with a post calcination treatment (Fig. 1) [23]. In a typical procedure, a mixture of $NiCl_2.6H_2O$, $CoCl_2.6H_2O$, Urea and NH_4F were dissolved in 35 mL of deionized water with the aid of magnetic stirrer. The molar ratio of Ni^{2+}/Co^{2+}/Urea/NH_4F was fixed at 1/2/15/6. A piece of Ni Foam was then put into obtained solution, before transferring to a 50-ml Teflon-lined autoclave. The reaction was carried out at 120°C for 6 hours. The $NiCo_2O_4$ coated Ni-foam was

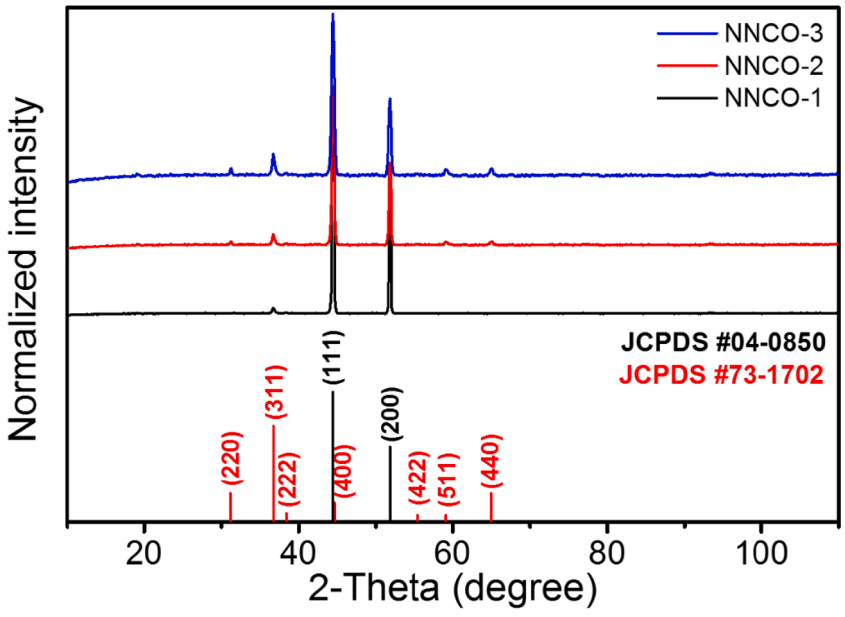

Fig. 2. XRD patterns of NNCO-1, NNCO-2 and NNCO-3 samples with the patterns of reference of $NiCo_2O_4$ (red bars) and Ni foam (black bars).

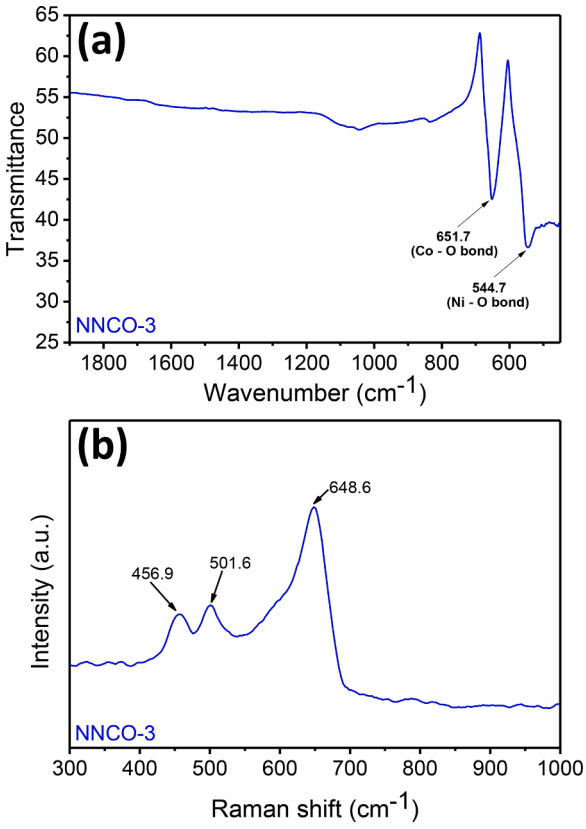

Fig. 3. (a) FT-IR result of the NNCO-3 material; **(b)** Raman spectra of the NNCO-3 material.

collected and washed with deionized water and ethanol several times before calcined at 300°C in air for 3h. The effect of composition on electrochemical property was investigated by changing the molar ratio of Ni^{2+}/Co^{2+}/Urea/NH_4F shown in **Table 1**.

2.3. Characterization

All synthesized materials were characterized by X-ray diffraction (XRD, Siemens D5005 X-ray diffract meter with Cu-Kα radiation); Fourier transform infrared (FTIR/ Perkin-Elmer Spectrum Two spectrometer), Raman spectra (Raman/Horiba Jobin - Yvon LabRam HR800 Raman spectrometer equipped); Scanning electron microscopy and energy-dispersive X-ray spectroscopy (SEM-EDS, JEOL JSM-6490 scanning electron microscope), Inductively coupled plasma (ICP, Optima 7300DV).

The electrochemical properties of all materials were performed on Metrohm Autolab PGSTAT 302N using cyclic voltammetry (CV) and galvanostatic charge - discharge (GCD) measurements. All electrochemical measurements were conducted using the standard three-electrode system consisting of working electrode, reference electrode (Ag/AgCl in 3M KCl solution) and counter electrode (Pt, sheet) in 3M KOH electrolyte. The working electrode of all $NiCo_2O_4$ material supported on Ni foam (NNCOs) were used directly with coating area 1.0×1.0 cm^2. The mass loading of active materials for NNCO-1, NNCO-2, NNCO-3, and NNCO-4 were approximately 0.77, 1.52, 3.14, and 0.56 mg/cm^2, respectively. The specific capacities (C_s) of materials were calculated from the CV and GCD curves follow the formula $Cs = (\int I\,dt)/(m\Delta)$, $C_s = (I\,\Delta t)/(m)$, respectively. Where, I is the discharge current (A), Δt is discharge time (sec), and m is the weight of active material in the electrode (g).

3. Results and discussion

3.1. Structural and morphological characterization

The crystal structure of $NiCo_2O_4$ supported on Ni foam were confirmed by X-ray diffraction and the result showed in **Fig. 2**. As shown in Fig. 2, the XRD patterns of all as-prepared materials shown two strong peaks located at 44.48 and 51.81°, which can be indexed to (111) and (200) planes belong to the Ni foam substrate (JCPDS #04-0850) [23–25]. The XRD peaks of the NNCO-3 sample located at 31.13, 36.76, 38.45, 44.61, 55.47, 59.15, 65.03° can be assigned to (220), (311), (222), (400), (422), (511), (440) planes of $NiCo_2O_4$ (JCPDS #73-1702)

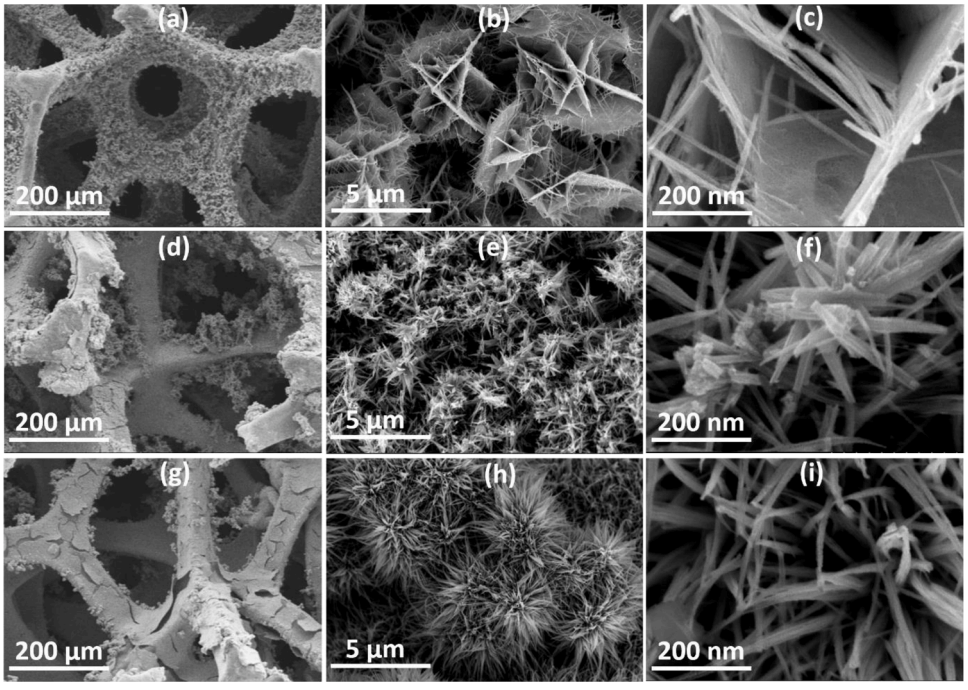

Fig. 4. SEM images of NNCO-1 **(a, b, c),** NNCO-2 **(d, e, f)** and NNCO-3 **(g, h, i).**

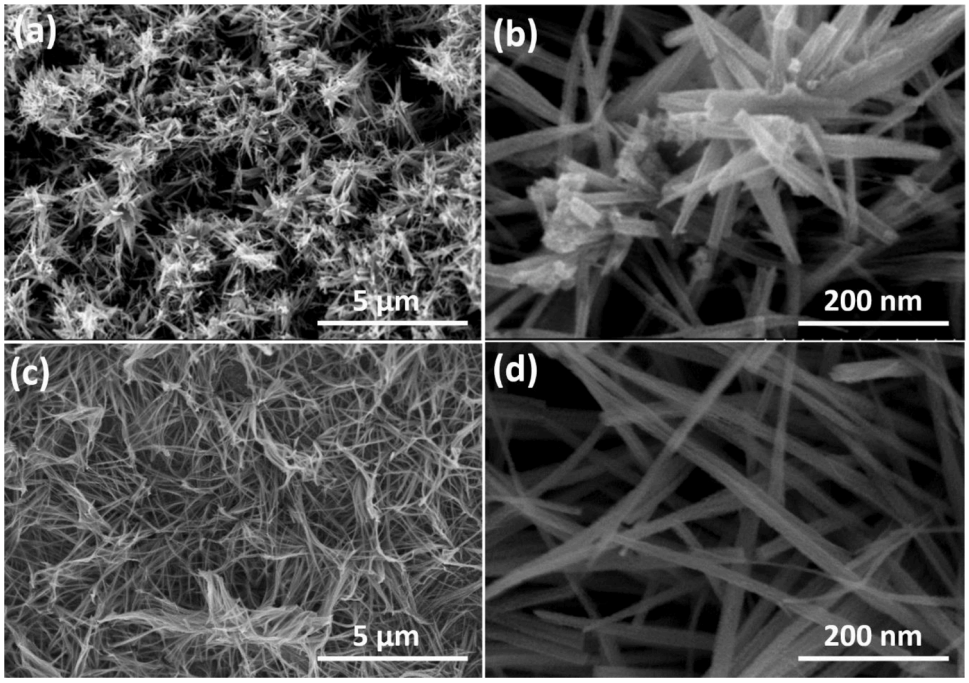

Fig. 5. SEM images of NNCO-2 **(a, b)** and NNCO-4 **(c, d).**

[26,27]. The diffraction intensity at the peaks decrease in the order NNCO-3 < NNCO-2 < NNCO-1 due the mass loading of $NiCo_2O_4$ on nickel foam decrease, respectively. Especially, the mass loading of active materials for NNCO-1, NNCO-2 and NNCO-3 were approximately 0.77, 1.52, and 3.14 mg/cm^2, respectively. These observations are similar to those of other the $NiCo_2O_4$ materials supported on Ni foam or cloth carbon [28,29]. Addition, in all XRD pattern no diffraction peaks of other phases, which indicated that synthesized $NiCo_2O_4$ and $NiCo_2O_4$ supported on Ni foam have been high purity.

The structure of $NiCo_2O_4$ supported on Ni foam were also proved by using the Raman spectra and the Fourier transform infrared (FT-IR) spectra. We chose NNCO-3 material to perform the measurement and the result shown in Fig. 3. In the FT-IR spectra of NNCO-3 material (Fig. 3a) appeared two sharp peaks located at frequencies of 544.7 cm^{-1} and 651.7 cm^{-1}, which can be indexed to the stretching vibrations of Ni-O and Co-O bonds in $NiCo_2O_4$ [30,31]. Addition, the Raman spectrum of the NNCO-3 material (Fig. 3b) shown three distinct peaks located 456.9, 501.6, and 648.6 cm^{-1}, which could be indexed to the E_g, F_{2g}, and A_{1g} vibration modes of the $NiCo_2O_4$ spinel structure [31,32].

The morphology of $NiCo_2O_4$ supported on Ni foam (NNCOs) shown in Figs. 4 and 5. Unexpectedly, the morphology of $NiCo_2O_4$ supported on Ni foam are completely different when the concentration of reaction precursors changed meanwhile the temperature and duration of the hydrothermal process is unchanged. As shown in Fig. 4, the morphology

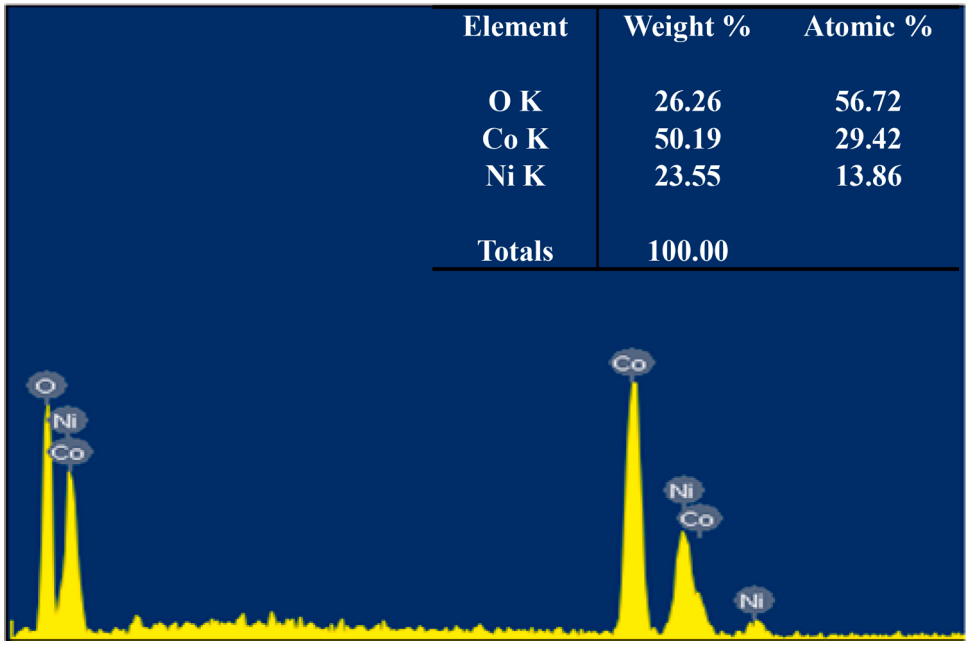

Fig. 6. The atomics ratio of the powder layer on NNCO-3 material.

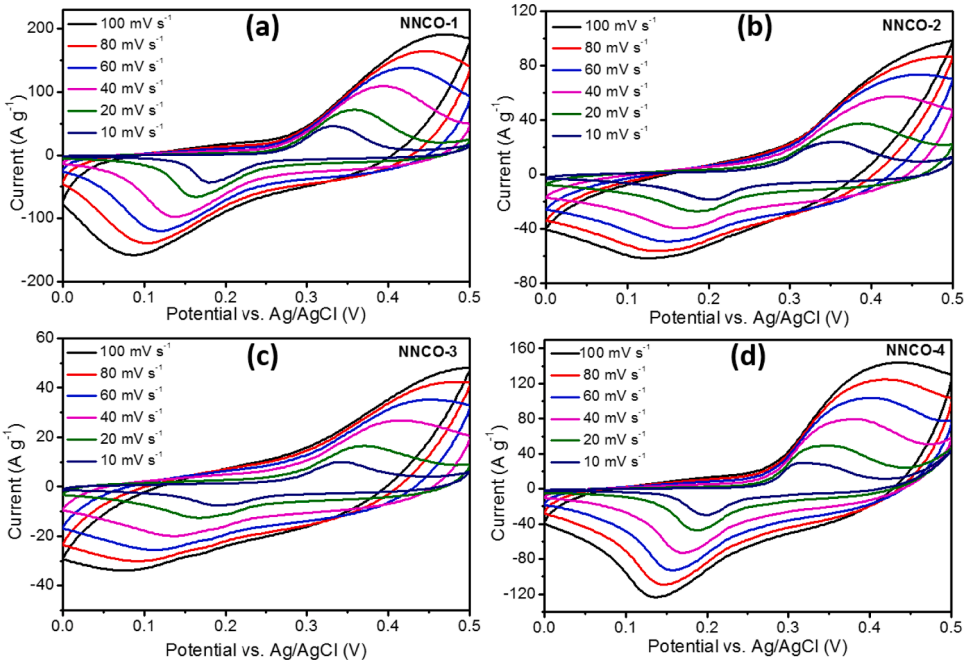

Figure 7. CV curves of all materials at different scan rate

of $NiCo_2O_4$ supported on nickel foam changed when the concentration of precursor changed. Specifically, when the synthesis process of $NiCo_2O_4$ supported on Ni foam at low precursor concentration (0.5/1/7.5/3), synthesized material (NNCO-1) has nanosheet-like with a thickness of about 25 to 30 nm and these as-formed nanosheets are intercrossed with each other. Meanwhile, when increase precursor concentration, the morphology of synthesized materials have nanorod structure with width of 25-30 nm (NNCO-2) and natural grass-like structure (NNCO-3). The NNCO-4 sample was synthesized with the same amount of precursor as NNCO1 sample (except urea). Fig. 5 shows that NNCO-4 sample has nanorod structure like NNCO-2 sample, its width is also about 25-30 nm. However, the morphology of NNCO-2 and NNCO-4 samples has been different about length of nanorods; specifically, the length of the NNCO-4 nanorods was longer than that of NNCO-2.

These observations indicate that the precursor concentration has a strong influence on the morphology of materials, which influences to the electrochemical efficiency. Compare to the $NiCo_2O_4$ material with the morphology as nanoparticles, microspheres [22,33], the as-prepared $NiCo_2O_4$ materials supported on nickel foam has mesoporous structure and higher the specific surface area, which provide low-resistance and more active sites leading to enhanced electron transfer and electrochemical performance [26,34–36].

The morphological differences of $NiCo_2O_4$ supported on Ni foam samples (NNCOs) can be attributed to differences in pH during hydrothermal process and concentration of precursors [37–40]. At a temperature of 120°C, the urea decomposes into ammonia (NH_3), which determines the pH of the solution. The NNCO-3 material was synthesized with the highest concentration of Ni^{2+}, Co^{2+}, and Urea leading to the precipitation of $NiCo_2O_4$-precursors which occurs rapidly. This confirmed through of the $NiCo_2O_4$ mass loading on Ni foam being the highest (3.14 mg/cm^2); small amount of $NiCo_2O_4$-precursor supported on nickel foam was removed during washing product; even when calcined at 300°C to created $NiCo_2O_4$, there is still $NiCo_2O_4$ powder falling out of nickel foam. These observations provide evidence the connection between the $NiCo_2O_4$ material layer and Ni foam in the NNCO-3 material is not sustainable and suggestion that the NNCO-3 material is not suitable as an energy storage electrode for the devices working under the shock and motion conditions. Conversely, the precipitation process of $NiCo_2O_4$ precursor when synthesized at low Ni^{2+}, Co^{2+} and Urea concentration occurs slowly, leading to the $NiCo_2O_4$ material layer on nickel foam is more homogeneous and more stable. Furthermore, the formation of the gas molecules leads to the higher pressure in the hydrothermal process is also different, it is expected that the growth of nanocrystals will be disturbed and thus may bring about the different about morphological differences when of the precursors is changed.

The ratio of Ni, Co and O atomics in the as-synthesized materials was confirmed by energy dispersive X-ray spectroscopy (EDS) analysis. The EDS measurement was conducted on the $NiCo_2O_4$ powder, which was obtained by removing carefully the $NiCo_2O_4$ layer on the NNCO-3 material, the result shown in Fig. 6. The EDS result of $NiCo_2O_4$ powder confirmed the existence of Ni, Co and O with atomic ratio of 1: 2.12: 4.09 and the absence of impurities, which is close to chemical formula of $NiCo_2O_4$. Moreover, the inductively coupled plasma (ICP) analysis results of the also confirmed the present of Ni, Co with atomic ratio of 1: 2.5, and the results were consistent. The XRD, FT-IR, Raman spectra, SEM, ICP, and EDS results confirmed that, the $NiCo_2O_4$ materials supported on Ni foam were successfully synthesized with different morphology. We hope that, the $NiCo_2O_4$ crystal growth on nickel foam leading to enhance the electrochemical performance compared to the pristine $NiCo_2O_4$ materials.

3.2. Electrochemical characteristics

3.2.1. CV analysis

The energy storage mechanisms of all materials was confirmed by cyclic voltammetry analysis within the potential range of 0 to 0.5 V at different scan rates. **Fig. 8a** shows CV curves of as-prepared materials at a scan rate of 10 mV s^{-1}, these is a pair of clear redox peaks located at about 0.19 V/0.38 V in all of the CV curves, which is attributed to redox reactions involved in $A-O/A-O-OH$ (A = Ni, Co) conversions [18,41,42]. This observation demonstrates that all composites exhibit the behavior of batteries and their main mechanism for storing energy based on redox reactions [14,20]. In a potential window of 0 to 0.5 V in an alkaline solution, redox reaction between $NiCo_2O_4$ and OH^- ion of KOH electrolyte can be described by the following equations:

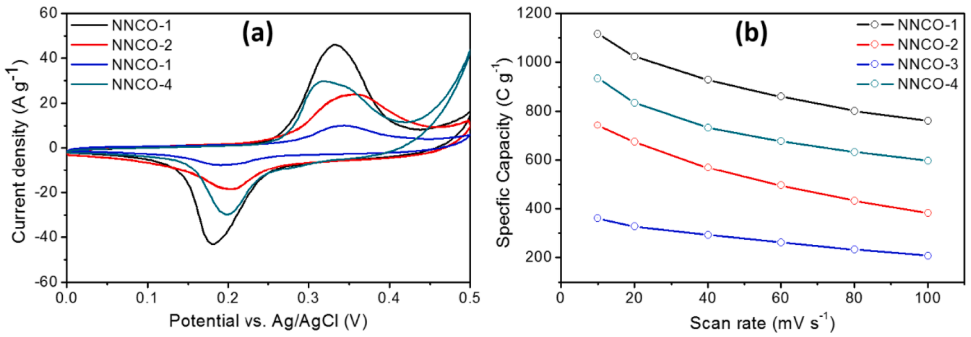

Fig. 8. **(a)** CV curves of all materials at a scan rate of 10 mV s^{-1}, **(b)** Specific capacity of all materials at different scan rates.

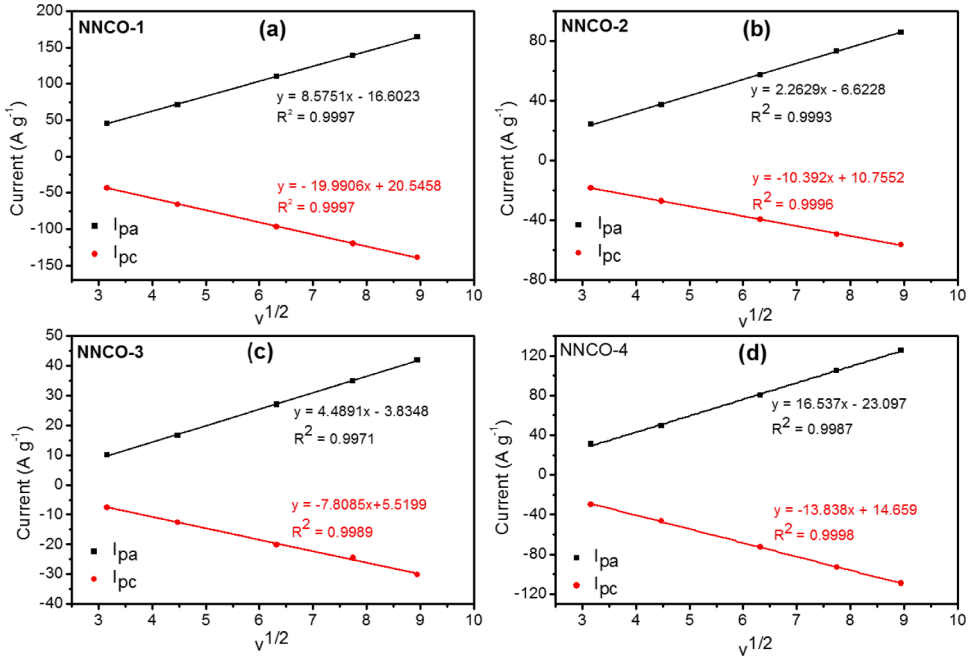

Fig. 9. Randles-Sevcik plots of $NiCo_2O_4$ supported on Ni foam.

$$NiCo_2O_4 + OH^- + H_2O \leftrightarrow NiOOH + 2CoOOH + e^- \quad (1)$$

$$CoOOH + OH^- \leftrightarrow CoO_2 + H_2O + e^- \quad (2)$$

Fig. 8a also indicated that the current density at redox peaks decreases in the order of NNCO-1 < NNCO-4 < NNCO-2 < NNCO-3 suggest that the redox reaction between $NiCo_2O_4$ and OH^- ion on the surface of the NNCO-1 electrode happens faster than those the NNCO-2, NNCO-3, and NNCO-4 electrode. Addition, the CV curve of NNCO-1 has internal area higher than those NNCO-2, NNCO-3, and NNCO-4 samples suggesting a higher specific capacity of NNCO-1 material compared to that of other materials. Fig. 7(a-d) show CV curves at different scan rate of NNCO-1, NNCO-2, NNCO-3, and NNCO-4, respectively. As shown in Fig. 7, when the scan rate was increased from 10 - 100 mV s^{-1}, both the anode peak current (I_{pa}) and cathode peak current (I_{pc}) increase, this proved redox reaction of active material on electrode with OH^- ions of electrolyte occurs quickly [21,43]. However, the oxidation and reduction potentials were shifted to the left and right, respectively when the scan rate increased due the electrode polarization, which usually occurs in electrochemical batteries.

Observe the CV curves of NNCO-1, NNCO-2, NNCO-3, and NNCO-4 at the same scan rate found that, both I_{pa} and I_{pc} values decrease in the order NNCO-1 > NNCO-4 > NNCO2 > NMCO-3, suggest that NNCO-1 sample with morphology as nanosheet-like can higher store large than other morphologies. The specific capacity (C_s) of these materials at different scan rates was calculated from CV profiles, and the results shown in Fig. 8b. The specific capacity values of all materials increased with decreasing scan rate, and at the same scan rate the C_s values decrease in the order NNCO-1 > NNCO-4 > NNCO-2 > NNCO-3. The maximum and minimum specific capacity values of these materials obtained at 10 and 100 mV s^{-1}, respectively. Especially, the maximum/minimum specific capacity of NNCO-1 were calculated to be 1016.3/760 C g^{-1}, much higher than that of NNCO-2 (743/381 C g^{-1}), NNCO-3 (324/208 C g^{-1}), and NNCO-4 (935/597.6 C g^{-1}). Thus, although all as-prepared material have the same characteristic properties but their electrochemical performance is very different. These observations suggestion that the morphology has a strong influence on the electrochemical properties of materials. In addition, the anodic and cathodic peaks shift to higher and lower potentials respectively as the scan speed increased, this is due to the low material resistance and the fast ion diffusion rate during process reaction [43]. The variation of I_{pa} and I_{pc} values when the scan rate increase from 10 to 100 mV s^{-1} was also calculated from CV profiles, and the result shown in **Fig. 9(c-d)**. As shown in **Fig. 9**, both I_{pa} and I_{pc} vary linearly with the square root of the scan rate ($\nu^{1/2}$), comply the equation the Randles–Sevcik equation [44]. These observations provides evidence the redox reaction occurring at the electrode–electrolyte interface are fast and highly reversible and limited only by the diffusion of electrolytes [22]. According to Randles–Sevcik equation, when the CV measurements were performed under the same conditions, the variation of I_{pa} and I_{pc} depends diffusion

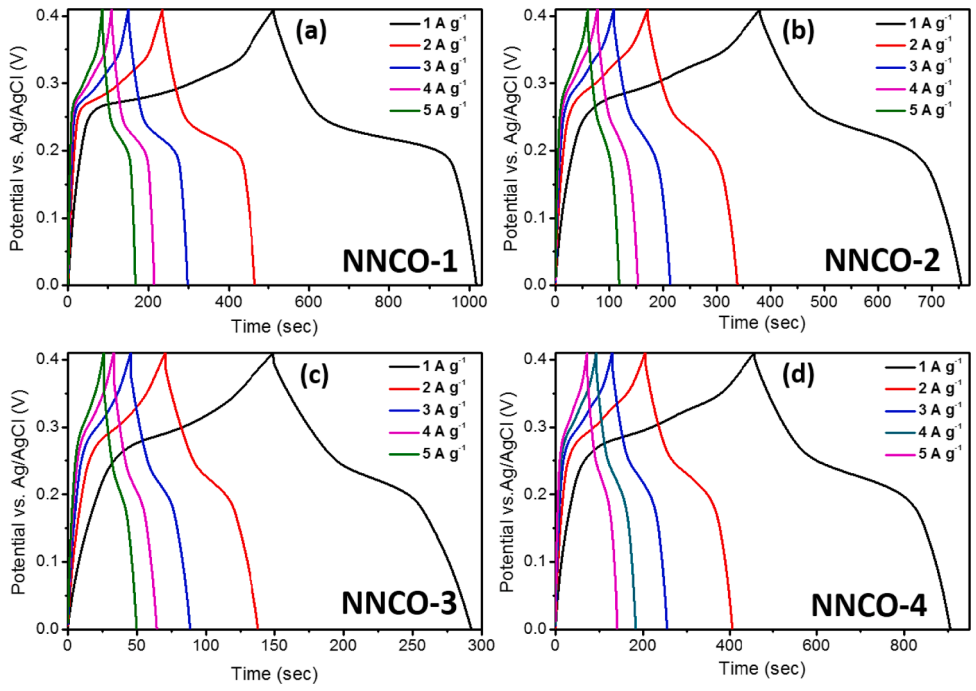

Fig. 10. GCD profiles of the NNCO-1, NNCO-2, NNCO-3, and NNCO-4 samples at different current density.

Table 2
Comparison of $NiCo_2O_4$-based electrode materials for hybrid supercapacitors.

Electrode Material	Method of synthesis	Electrolyte	C_s from GCD	Reference
$NiCo_2O_4$ nanoflowers	Hydrothermal	6 M KOH	122.5 C g^{-1} at 1 A g^{-1}	[46]
$NiCo_2O_4$ hollow spheres	Hydrothermal	3 M KOH	171.2 C g^{-1} at 1 A g^{-1}	[47]
$NiCo_2O_4$ microspheres	Co-precipitation	6 M KOH	202 C g^{-1} at 1 A g^{-1}	[22]
Mn-doped $NiCo_2O_4$	Hydrothermal	3 M KOH	204.3 C g^{-1} at 1 A g^{-1}	[33]
rGO@$NiCo_2O_4$	Hydrothermal	3 M KOH	427 C g^{-1} at 1 A g^{-1}	[21]
NNCO-2	Hydrothermal	3 M KOH	374.5 C g^{-1} at 1 A g^{-1}	This study
NNCO-1	Hydrothermal	3 M KOH	503.5 C g^{-1} at 1 A g^{-1}	This study

coefficient of electrolyte ion. The above analysis suggestion the I_{pa} and I_{pc} of NNCO-1 higher than those NNCO-2, NNCO-3, and NNCO-4 may be due to the diffusion coefficient of OH^- ion for the NNCO-1 electrode is higher compared to other electrodes.

3.2.2. GCD and cycling analysis

Fig. 10**(a-d)** show GCD profiles at different current density from 1 to 5 A g^{-1} within the potential range of 0 to 0.41 V of NNCO-1, NNCO-2, NNCO-3, and NNCO-4, respectively. As shown in Fig. 10, the GCD profiles of all as-prepared materials is the same due they have the same material nature. The discharge profiles show a voltage plateaus located at about 0.2V, which was appropriate to the position of cathodic peak in the CV curves. A clear voltage plateau also appeared at about 0.28V in the charge profiles, which corresponding to the voltage of anodic peak was observed in the CV curves. The difference between the discharge and charge potential plateau in the GCD profiles is very little suggestion that high electrochemical reversibility [18,45]. Addition, the voltage plateaus little changed when the density current increased from 1 to 5 A g^{-1}, this provides evidence the electrode polarization in the charge-discharge process of all materials is small even when the charge/discharge process at high density current.

The specific capacity (C_s) of material were calculated from GCD profiles and the result shown in Fig. 12**a**. As expected of the storage capacity from CV analysis result, C_s of NNCO-1 always higher than other materials when comparing at the same current density and the C_s values decrease in the order NNCO-1 > NNCO-4 > NNCO-2 > NMCO-3. Specifically, at a current density of 1 A g^{-1}, the C_s of NNCO-1 is 503.5 C g^{-1}, much higher than that of NNCO-2 (374.5 C g^{-1}), NNCO-3 (143.5 C g^{-1}), and NNCO-4 (449.3 C g^{-1}). For comparison, the C_s of several battery-type electrodes fabricated base the $NiCo_2O_4$ nanomaterials for application in hybrid supercapactiors were summarized in Table 2. The maximum specific capacity of NNCO-1 material was 503.5 C g^{-1} at a density current of 1 A g^{-1}, which was much higher than that of $NiCo_2O_4$ nanoflowers (122.5 C g^{-1}) [46], $NiCo_2O_4$ hollow spheres (171.2 C g^{-1}) [47], Mn-doped $NiCo_2O_4$ (204.3 C g^{-1}) [33], rGO@$NiCo_2O_4$ nanocomposites (427 C g^{-1}) [21] . The match well between the CV and GCD results may conclude that, the morphology of materials is an important determinant to their electrochemical performance. The difference about electrochemical performance mainly comes from the difference of material resistance, surface area and ion diffusion rate [22,48] . As shown in SEM image (Fig. 4 and Fig. 5), $NiCo_2O_4$ supported on Ni Foam materials with morphology nanosheet-like (NNCO-1) have ion diffusion rate are higher than those nanorod-like (NNCO-2, NNCO-4) and natural grass-like (NNCO-3) [20,48]. Thus, control the morphology of the material is a direct and forceful strategy to alter the electrochemical properties of material. We hope that, the NNCO-1 material is a promising material for application as battery-type electrode in hybrid supercapacitors.

The cycle capability is an important parameter for materials used as electrode in hybrid supercapacitors. To evaluate the cycle capability, GCD measurement was performed continuously 2000 cycle at a current density of 2 A g^{-1} and the result shown in Fig. 12**b**. It can see that, the cycling performance of all materials is quite similar due they have the same material nature. After 2000 consecutive cycles all synthesized materials maintained 95-97 % of the original C_s. Specifically, the cycling performance decreases in the order NNCO-1 (97.25%) > NNCO-4 (96.5%) > NNCO-2 (95.7%) > NNCO-3 (95.66%). The results showed that, morphology not only effects to the specific capacity, but also the cycling performance. The enhancement of the cycling efficiency of

Table 3
Values of circuit elements in the EIS equivalent circuit.

Materials/Parameters	NNCO-1	NNCO-2	NNCO-3	NNCO-4
R_s (mΩ)	693	718	803	708
R_{ct} (mΩ)	76	414	555	342
C (mF)	1.46	0.13	0.23	0.9
W (mMho)	1.66	115	442	324
CPE (mMho)	43.6	174	251	79.2
	N = 0.964	N = 1.08	N = 1.04	N = 1.01

NNCO-1 compared to NNCO-2, NNCO-3, and NNCO-4 is due to the fact that the nanosheet-like NNCO-1 sample has lower resistance and better diffusion rate (Table 3), which decided to the reversibility of the redox reaction on the electrode surface. The morphology of all materials after 2000 charge/discharge cycles was also examined by scanning electron microscopy analysis and the results showed in Fig. 11. As shown in Fig. 11, the morphology of all materials do not change after continuous charging and discharging, suggestion that synthesized materials have a stable structure and the connection between layer $NiCo_2O_4$ and Ni foam is enduring. This maintaining high capacitance and morphological stability shows very little change of the spinel structure of $NiCo_2O_4$ as well as high reversibility in the charge/discharge reactions. Consider overall the electrochemical properties of all materials indicated that, NNCO-1 sample is a promising material for application as battery-type electrode in hybrid supercapcitor.

3.2.3. EIS analysis

To provide evidence more insight to the better electrochemical

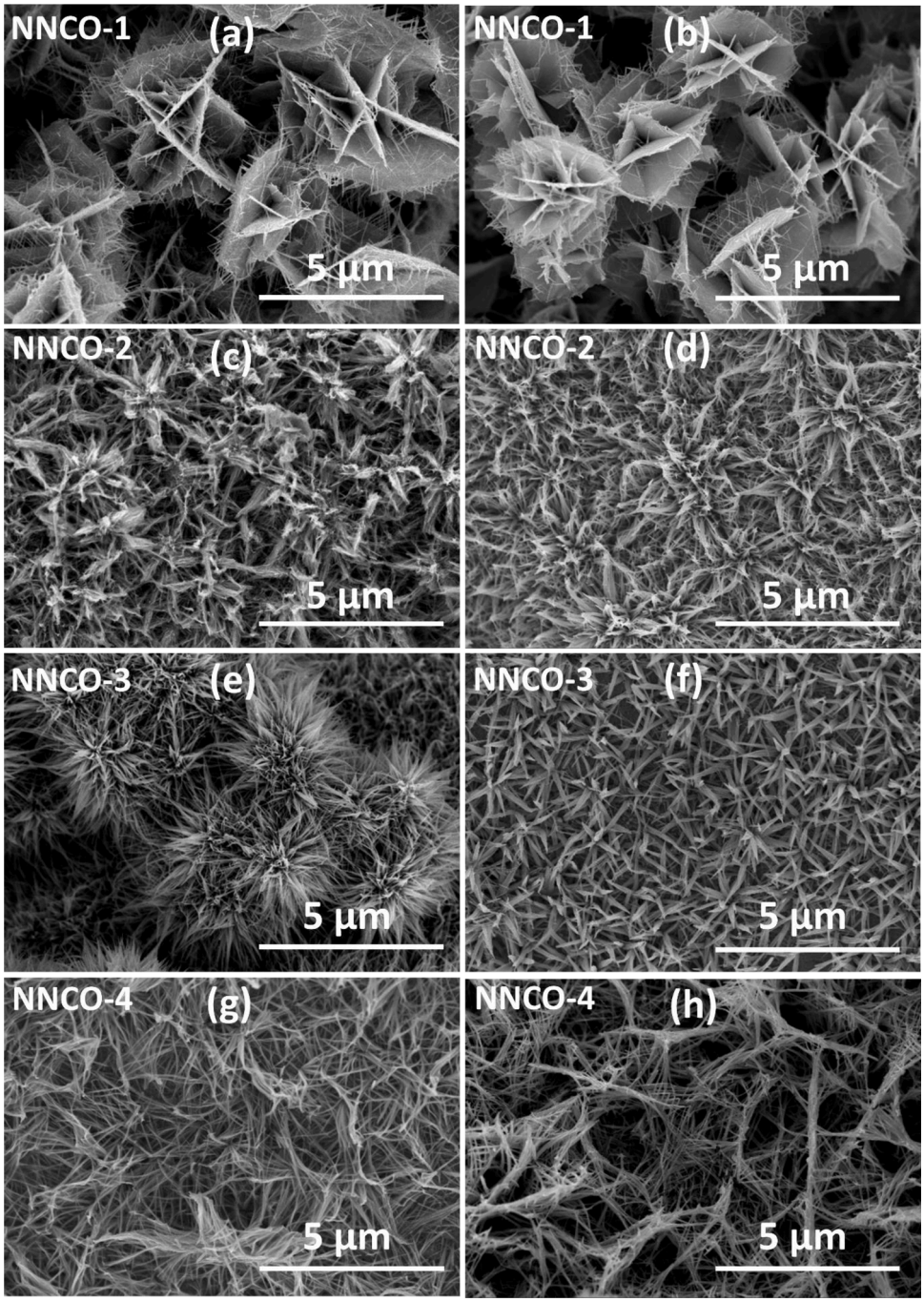

Fig. 11. SEM images of all materials before charge/discharge (**a, c, e, g**) and after 2000 cycle charge/discharge (**b, d, f, h**).

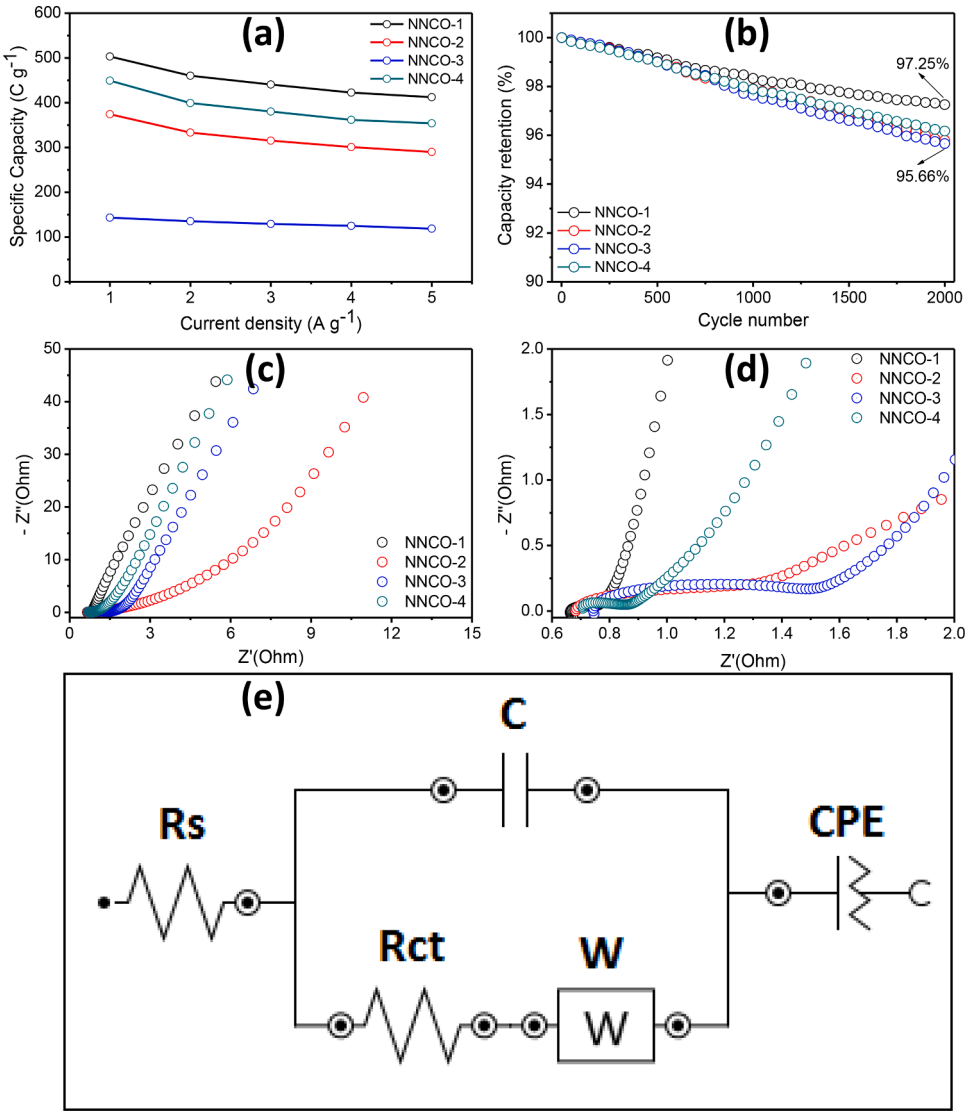

Fig. 12. **(a)** Specific capacity of all material at different current density, **(b)** Cycling performance of all materials after 2000 cycles at a current density of 2 A g^{-1}; **(c)** Overall Nyquist plots of the neat all materials; **(d)** Nyquist plots of all materials in the high-frequency region; **(e)** Equivalent circuit diagram used for fitting EIS data.

performances of the NNCO-1 material than those of the NNCO-2, NNCO-3, and NNCO-4 materials, EIS measurements were conducted in the frequency range of 10^{-2} to 10^{6} Hz with amplitude of 10 mV and the results are presented in Fig. 12**(c-d)**. As shown in Fig. 12**(c-d)**, the Nyquist plots of all as-prepared materials included of a very small depressed semicircle at high frequency and an inclined line at low frequency suggestion that the electrochemical behavior of the electrode materials is the same. At the high frequency region, the intercept of the semicircle in EIS spectra with the real axis depicts the equivalent series resistance (R_s), which is contributed from several factors including the resistance of the electrode material/current collector, the resistance of the bulk electrolyte solution, and the resistance of the electrode material [49]. Since we used the same procedure for preparation of the materials and the conditions for performing the EIS analysis are exactly the same, the difference in R_s is mainly originated from the resistance of the electrode materials. The equivalent circuit diagram used to calculate the impedance parameters was shown in Fig. 12**e**, and the parameter values were summarized Table 3.

As shown in Table 3, the R_s values of NNCO-1, NNCO-2, NNCO-3, and NNCO-4 materials are 0.693, 0.718, 0.803, 0.708 Ω, respectively. This values was very little, which provides evidence the voltage drop phenomenon (Fig. 10) immediately after the start of the discharge process is small. In the equivalent circuit diagram, the R_{ct}, W, and CPE parameters are related to the charge-transfer resistance, the heterogeneity of the electrode surface, diffusion rate of electrolyte ion, respectively [32]. Table 3 also indicated that the values of all three parameters increase in the order NNCO-1 < NNCO-4 < NNCO-2 < NMCO-3, which corresponding to the electronic charge-transfer on NNCO-1 electrode surface is more convenient advantageous, the surface of NNCO-1 electrode is also more homogeneity, the OH- ion diffusion rate at near the NNCO-1 electrode surface is higher compared other electrodes [50]. The difference of the parameters in the equivalent circuit diagram mainly related to the morphology of materials. The EIS results provide evidence to explain why the electrochemical performance of the NNCO-1 material higher than other materials. Therefore, morphology controlled synthesis to obtain the material with the best performance is important for the battery-type electrode materials to application in hybrid supercapacitors.

4. Conclusions

In conclusion, by a facile hydrothermal method we were successfully synthesized $NiCo_2O_4$ supported on Ni foam with different morphology, where the reaction precursor concentration is crucial affected the

morphology of the materials. The research results of electrochemical properties indicated that the morphology of materials have strong influenced on their electrochemical performance. Specially, $NiCo_2O_4$ supported on Ni foam with nanosheet-like morphology (NNCO-1) exhibited superior electrochemical performance than different morphologies. At a same current of 1 A g^{-1}, the specific capacity (C_s) of NNCO-1 (nanosheet-like) is 503.5 C g^{-1} meanwhile, the C_s of NNCO-2 (nanorod-like), NNCO-3 (grass-like), and NNCO-4 (nanorod-like) are 374.5, 143.5, 449.3 C g^{-1}, respectively. The result of cycling test indicated that all materials exhibit excellent capacitance retention with the ability to maintain 95 to 97 % capacitance after 2000 discharge cycles at a current density of 2 A g^{-1}. All of the results shown that the NNCO-1 sample can be a promising material in the application of high performance hybrid supercapacitors.

CRediT authorship contribution statement

Doan Tien Phat: Conceptualization, Data curation, Formal analysis, Investigation, Methodology, Supervision, Validation, Visualization. **Pham Manh Thao:** Formal analysis, Investigation, Methodology, Supervision, Validation, Visualization, Writing - original draft, Writing - review & editing. **Nguyen Van Nghia:** Data curation, Formal analysis, Investigation, Methodology, Validation, Writing - original draft. **Luong Trung Son:** Formal analysis, Investigation, Methodology, Validation, Writing - review & editing. **Tran Viet Thu:** Formal analysis, Investigation, Methodology, Validation, Writing - original draft. **Ngo Thi Lan:** Formal analysis, Investigation, Methodology, Validation, Writing - original draft. **Ngo Quy Quyen:** Formal analysis, Investigation, Methodology, Validation, Writing - original draft. **Nguyen Van Ky:** Formal analysis, Investigation, Methodology, Validation, Writing - original draft. **To Van Nguyen:** Conceptualization, Data curation, Formal analysis, Investigation, Methodology, Supervision, Validation, Visualization, Writing - original draft, Writing - review & editing.

Declaration of Competing Interest

There are no conflicts of interest to declare.

References

[1] D. Li, et al., Core/shell Ni–P@Ni–Co composite with micro-/nanostructure for supercapacitor, J. Mater. Sci. (2018) 53.
[2] H. Yin, Z. Tang, Ultrathin two-dimensional layered metal hydroxides: an emerging platform for advanced catalysis, energy conversion and storage, Chem. Soc. Rev. 45 (18) (2016) 4873–4891.
[3] S. Dai, et al., A high-performance supercapacitor electrode based on N-doped porous graphene, J. Power Sources 387 (2018) 43–48.
[4] W. Xu, et al., Lithium metal anodes for rechargeable batteries, Energy Environ. Sci. 7 (2) (2014) 513–537.
[5] A. González, et al., Review on supercapacitors: Technologies and materials, Renewable Sustainable Energy Rev. 58 (2016) 1189–1206.
[6] T. Kim, et al., Lithium-ion batteries: outlook on present, future, and hybridized technologies, J. Mater. Chem. A 7 (7) (2019) 2942–2964.
[7] A. Mahmoudzadeh Andwari, et al., A review of Battery electric vehicle technology and readiness levels, Renewable Sustainable Energy Rev. 78 (2017) 414–430.
[8] A. Makhdoomi, et al., A review on recent advances in hybrid supercapacitors: design, fabrication and applications, Renewable Sustainable Energy Rev. 101 (2019) 123–145.
[9] W. Zuo, et al., Battery-supercapacitor hybrid devices: recent progress and future prospects, Adv. Sci. 4 (2017), 1600539.
[10] S. Dai, et al., Controlled synthesis of three-phase NixSy/rGO nanoflake electrodes for hybrid supercapacitors with high energy and power density, Nano Energy 33 (2017) 522–531.
[11] B. Zhao, et al., Rational design of nickel hydroxide-based nanocrystals on graphene for ultrafast energy storage, Adv. Energy Mater. (2017), 1702247.
[12] A. Vlad, et al., Hybrid supercapacitor-battery materials for fast electrochemical charge storage, Sci. Rep. 4 (2014) 4315.
[13] A. Afif, et al., Advanced materials and technologies for hybrid supercapacitors for energy storage – a review, J. Energy Storage 25 (2019), 100852.
[14] W. Jiang, et al., Investigation on electrochemical behaviors of $NiCo_2O_4$ battery-type supercapacitor electrodes: the role of aqueous electrolyte, Inorg. Chem. Front. (2017) 4.
[15] R. Blueocean, Y. Kim, H. Yoon, Electrical and electrochemical properties of conducting polymers, Polymers 9 (2017) 150.
[16] J. Xiao, S. Yang, Sequential crystallization of sea urchin-like bimetallic (Ni, Co) carbonate hydroxide and its morphology conserved conversion to porous $NiCo_2O_4$ spinel for pseudocapacitors, RSC Adv. 1 (4) (2011) 588–595.
[17] T.-Y. Wei, et al., A cost-effective supercapacitor material of ultrahigh specific capacitances: spinel nickel cobaltite aerogels from an epoxide-driven sol-gel process, Adv. Mater. 22 (2010) 347–351. Deerfield Beach, Fla.
[18] H. Wang, Q. Gao, L. Jiang, Facile approach to prepare nickel cobaltite nanowire materials for supercapacitors, Small (2011) 7. Weinheim an der Bergstrasse, Germany.
[19] H. Zhou, et al., RGO/MnO_2/polypyrrole ternary film electrode for supercapacitor, Mater. Chem. Phys. (2016) 177.
[20] J. Fang, et al., Morphology tuned synthesis of battery-type $NiCo_2O_4$ for high performance hybrid supercapacitors, J. Alloys Compd. (2019) 804.
[21] A. Mondal, et al., Large-scale synthesis of porous $NiCo_2O_4$ and rGO-$NiCo_2O_4$ hollow-spheres with superior electrochemical performance as faradaic electrode, J. Mater. Chem. A 5 (2017) 16854–16864.
[22] H. Fu, et al., Designed formation of $NiCo_2O_4$ with different morphologies self-assembled from nanoparticles for asymmetric supercapacitors and electrocatalysts for oxygen evolution reaction, Electrochim. Acta (2018) 296.
[23] H. Wan, et al., Nickel nanowire@porous $NiCo_2O_4$ nanorods arrays grown on nickel foam as efficient pseudocapacitor electrode, Front. Energy Res. (2017) 5.
[24] H.-W. Wang, X. Wang, Growing nickel cobaltite nanowires and nanosheets on carbon cloth with different pseudocapacitive performance, ACS Appl. Mater. Interfaces (2013) 5.
[25] Q. Wang, et al., $NiCo_2O_4$ nanowire arrays supported on Ni foam for high-performance flexible all-solid-state supercapacitors, J. Mater. Chem. A (1) (2013).
[26] H. Rong, et al., Hierarchical $NiCo_2O_4$ @$NiCo_2S_4$ nanocomposite on Ni foam as an electrode for hybrid supercapacitors, ACS Omega 3 (2018) 5634–5642.
[27] Z. Yanjun, et al., Facile fabrication of hierarchical porous rose-like $NiCo_2O_4$ nanoflake/$MnCo_2O_4$ nanoparticle composite with enhanced electrochemical performance for energy storage, J. Mater. Chem. A (2015) 3.
[28] G. Chen, et al., Hierarchical $NiCo_2O_4$ nanowire arrays on Ni foam as an anode for lithium-ion batteries, RSC Adv. 5 (29) (2015) 23067–23072.
[29] Qin, G., et al., Hierarchically porous Ni monolith@branch-structured NiCo2O4 for high energy density supercapacitors. ArXive, 2016. 26.
[30] B. Wang, et al., Rapid synthesis of rGO conjugated hierarchical $NiCo_2O_4$ hollow mesoporous nanospheres with enhanced glucose sensitivity, Nanotechnology 28 (2017), 025501.
[31] V.-N. Nguyen, et al., Facile synthesis of a $NiCo_2O_4$ nanoparticles mesoporous carbon composite as electrode materials for supercapacitor, ChemistrySelect 5 (2020) 7060–7068.
[32] H. Nguyen, et al., Mixing amorphous carbon enhanced electrochemical performances of $NiCo_2O_4$ nanoparticles as anode materials for sodium-ion batteries, Appl. Phys. A (2020) 126.
[33] T.V. Nguyen, et al., Facile synthesis of Mn-doped $NiCo_2O_4$ nanoparticles with enhanced electrochemical performance for a battery-type supercapacitor electrode, Dalton Trans. 49 (20) (2020) 6718–6729.
[34] N. Feng, et al., Growth of nanostructured nickel sulfide films on Ni foam as high-performance cathodes for lithium ion batteries, Phys. Chem. Chem. Phys. (15) (2013).
[35] G. Gao, et al., Hierarchical $NiCo_2O_4$ nanosheets grown on Ni nanofoam as high-performance electrodes for supercapacitors, Small (2015) 11. Weinheim an der Bergstrasse, Germany.
[36] W. Jian, et al., Ultrathin $NiCo_2O_4$ nanosheets grown on three-dimensional interwoven nitrogen-doped carbon nanotubes as binder-free electrodes for high-performance supercapacitors, J. Mater. Chem. A (3) (2015).
[37] D. Guragain, et al., Influence of urea on the synthesis of $NiCo_2O_4$ nanostructure: morphological and electrochemical studies, J. Nanosci. Nanotechnol. 20 (2019) 2526–2537.
[38] A.P.A. Faiyas, et al., Dependence of pH and surfactant effect in the synthesis of magnetite (Fe_3O_4) nanoparticles and its properties, J. Magn. Magn. Mater. 322 (2010) 400–404.
[39] W. Ramadan, et al., Effect of pH on the Structural and magnetic properties of magnetite nanoparticles synthesised by co-precipitation, Adv. Mate. Res. 324 (2012) 129–132.
[40] G. Amin, et al., Influence of pH, precursor concentration, growth time, and temperature on the morphology of ZnO nanostructures grown by the hydrothermal method, J. Nanomater. 2011 (2011), 269692.
[41] Y. Li, et al., Review and prospect of $NiCo_2O_4$-based composite materials for supercapacitor electrodes, J. Energy Chem. 31 (2019) 54–78.
[42] Z. Wu, Y. Zhu, X. Ji, $NiCo_2O_4$-based materials for electrochemical supercapacitors, J. Mater. Chem. A 2 (36) (2014) 14759–14772.
[43] P. Xu, et al., Carbon nanotube fiber based stretchable wire-shaped supercapacitors, Adv. Energy Mater. (4) (2014).
[44] H. Wei, et al., Electrochromic polyaniline/graphite oxide nanocomposites with endured electrochemical energy storage, Polymer 54 (2013) 1820–1831.
[45] J. Ren, et al., Flexible and weaveable capacitor wire based on a carbon nanocomposite fiber, Adv. Mater. (2013) 25. Deerfield Beach, Fla.
[46] W. Jiang, et al., Investigation on electrochemical behaviors of $NiCo_2O_4$ battery-type supercapacitor electrodes: the role of an aqueous electrolyte, Inorg. Chem. Front. 4 (10) (2017) 1642–1648.
[47] A. Mondal, et al., Large-scale synthesis of porous $NiCo_2O_4$ and rGO–$NiCo_2O_4$ hollow-spheres with superior electrochemical performance as a faradaic electrode, J. Mater. Chem. A 5 (32) (2017) 16854–16864.

[48] H. Cheng, et al., Effect of phase composition, morphology, and specific surface area on the photocatalytic activity of TiO_2 nanomaterials, RSC Adv. 4 (87) (2014) 47031–47038.

[49] B.-A. Mei, et al., Physical interpretations of Nyquist plots for EDLC electrodes and devices, J. Phys. Chem. C 122 (1) (2018) 194–206.

[50] Y. Lei, et al., Rapid microwave-assisted Green synthesis of 3D hierarchical flower-shaped $NiCo_2O_4$ microsphere for high-performance supercapacitor, ACS Appl. Mater. Interfaces 6 (3) (2014) 1773–1780.